American Mineralogist, Volume 69, pages 165–175, 1984

Thermodynamic analysis of the system $CaCO_3$–$MgCO_3$ in the tetrahedron approximation of the Cluster Variation Method

BENJAMIN BURTON[1] AND RYOCHI KIKUCHI[2]

Department of Earth and Space Sciences
State University of New York, Stony Brook, New York 11794

Abstract

A thermodynamic model of phase relations in the system $CaCO_3$–$MgCO_3$ is presented. The model is based on the tetrahedron-approximation in the Cluster Variation Method, for a trigonally distorted face-centered-cubic (fcc) Ising lattice. We treat dolomite [$CaMg(CO_3)_2$] type ordering as the separation of species-1 and -2 atoms onto alternate fcc-(111) → hexagonal-(000*l*) planes and relate this ordering to an intersublattice pseudopair-wise energy parameter ($\epsilon_{ier} < 0$). we also consider intrasublattice interactions associated with the energy parameter ($\epsilon_{ira} > 0$) and relate these interactions to exsolution. For stoichiometric dolomite, we compare the tetrahedron-approximation to a Bragg–Williams approximation for calculation of the stabilization energy, from experimental brackets for the critical temperature of cation disordering (T_c). We demonstrate that the tetrahedron-approximation gives a better result for the stabilization energy precisely because it includes short-range order (SRO), and we note that it predicts considerable SRO above T_c. For the segment calcite–dolomite, our calculated diagram (for $R\epsilon \equiv -\epsilon_{ira}/\epsilon_{ier} = 6$) is in qualitative to semiquantitative agreement with the experimental diagram of Goldsmith and Heard (1961). With just the two parameters ϵ_{ier} and ϵ_{ira} the theoretical diagram is symmetric about the dolomite composition and with three parameters an asymmetric diagram can be obtained. For the segment dolomite–magnesite, the model is inadequate in some respects, and we note that another configurational degree of freedom is required to achieve full qualitative agreement between the calculated and experimental diagrams for this region.

Introduction

Binary phase diagrams of the type shown in Figure 1, or related diagrams, have been proposed for a number of mineral systems (Table 1). Characteristic features of Figure 1 are: (1) a line λ indicating a transition higher than first-order in character (first-order in the sense of Ehrenfest); between a high-temperature higher symmetry phase α and a low-temperature lower symmetry phase β. (2) two-phase fields in which α and β coexist at low temperatures. (3) tricritical points, $\{X_3, T_3\}$ and $\{X_{3'}, T_3'\}$, where the curve λ intersects the two-phase fields.

The main purpose of this paper is to show, with the system $CaCO_3$–$MgCO_3$ as an example, that the macroscopic phase relations represented in Figure 1 are predicted directly by an Ising model-type calculation based on the tetrahedron-approximation in the cluster variation method, CVM (Kikuchi, 1951). With this calculation, we achieve qualitative to semiquantitative agreement with experiment for the Ca-rich side of the diagram, and our results lead to a particularly simple physical interpretation for the relationship between energy parameters and observed phase relations.

The tetrahedron-approximation gives a very detailed account of the equilibrium state of order including the long-range order (LRO) parameter (S_{LRO}), and short range order (SRO) parameters for near neighbor (nn-) cation pairs, triangles, and tetrahedra. Inclusion of SRO is an essential difference between the CVM approach and other proposed models for systems of this kind (Navrotsky and Loucks, 1977; Merkel and Blencoe, 1982), and a second purpose of this paper is to discuss the advantages of including SRO in the theory. Another fundamental difference is that the CVM explicitly includes considerations of crystal geometry and symmetry that are ignored in the other models. Specifically, because of this difference, the CVM tetrahedron-approximation yields a topologically correct phase diagram for the Cu–Au system (van Baal, 1973, and Kikuchi, 1974), but a Bragg-Williams approximation (the approximation made in the models listed above and in regular-type solution models) yields a topologically incorrect diagram (Shockley, 1938). This metallurgical example should serve as a warning to

[1] Present address: Inorganic Materials Division, National Bureau of Standards, Washington, D.C. 20234.

[2] Present address: Hughes Research Laboratories, 3011 Malibu Canyon Road, Malibu, California 90265.

0003–004X/84/0102–0165$02.00

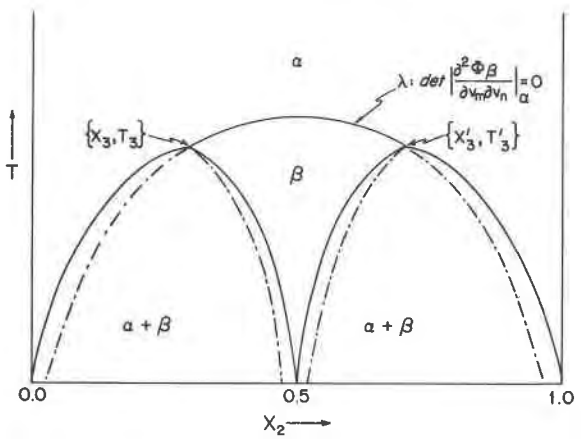

Fig. 1. Idealized phase diagram for $CaCO_3$–$MgCO_3$ and related systems. Phase α is a high-temperature higher symmetry phase and β is a low-temperature lower symmetry phase. The curve-λ is a line of higher than first-order transition which, if second-order, is defined by the condition $\det[\partial^2\phi_{ord}/\partial v_m \partial v_n]_{dis} = 0$, where v_m and v_n define the state of LRO. Dot-dashed extensions of λ are the ordering spinodals (as in Allen and Cahn, 1976). $\{X_3, T_3\}$ and $\{X_3', T_3'\}$ are tricritical points below which the stability field for β is flanked by two phase fields.

the geological community that simple regular-type solution models may not always be adequate for modeling complicated ordering systems. Thus, the final purpose of this paper is to acquaint the community with the more powerful CVM theory.

Background

Experimental phase diagrams for the system $CaCO_3$–$MgCO_3$ (Fig. 6; Goldsmith and Heard, 1961; Goldsmith and Newton, 1969; Irving and Wyllie, 1975; Byrnes and Wyllie, 1981) and the analogous system $CdCO_3$–$MgCO_3$ (Goldsmith, 1972) are similar to Figure 1. End members and disordered solutions (space group $R\bar{3}c$) are analogous to phase α, and the ordered intermediate, dolomite ($CaMg(CO_3)_2$, space group $R\bar{3}$) is analogous to phase β. In the dolomite type of ordering, Ca^{++} and Mg^{++} preferentially occupy alternate (000l) planes (sublattice-α and sublattice-β, respectively), and the average M–O distance in Ca^{++} sites is larger than in Mg^{++} sites, 2.387Å and 2.081Å, respectively (Althoff, 1977). An important difference between Figure 1, and the experimental diagram is that the experimental critical temperature for disordering of dolomite (T_c) is lower than the consolute temperature for two phases on the Mg-rich side of the diagram ($T_{consolute}$). This creates some theoretical problems which we shall discuss later.

Table 1. Binary systems for which the relations shown in Fig. 1 have been proposed.

System	Mineral Names	References
$CaCO_3$-$MgCO_3$	calcite-magnesite	5,7
$CdCO_3$-$MgCO_3$	...	4
Fe_2O_3-$FeTiO_3$	hematite-ilmenite	1
$NaAlSi_2O_6$-$CaMgSi_2O_6$	jadeite-diopside	3
$NaAlSi_3O_8$-$CaAl_2Si_2O_8$	albite-anorthite	2
$NaAlSi_3O_8$-$KAlSi_3O_8$	albite-sanidine	6

References are: 1 = Burton and Kikuchi (1981); 2 = Carpenter (1981); 3 = Carpenter (1978); 4 = Goldsmith (1972); 5 = Goldsmith and Heard (1961); 6 = Merkel and Blencoe (1982).

The model

The $CaCO_3$–$MgCO_3$ cation sublattice is a trigonally distorted version of the face centered cubic (fcc) lattice in which one fcc-[111] direction has been shortened to become the hexagonal-[0001] direction (Fig. 2a). Thus, if

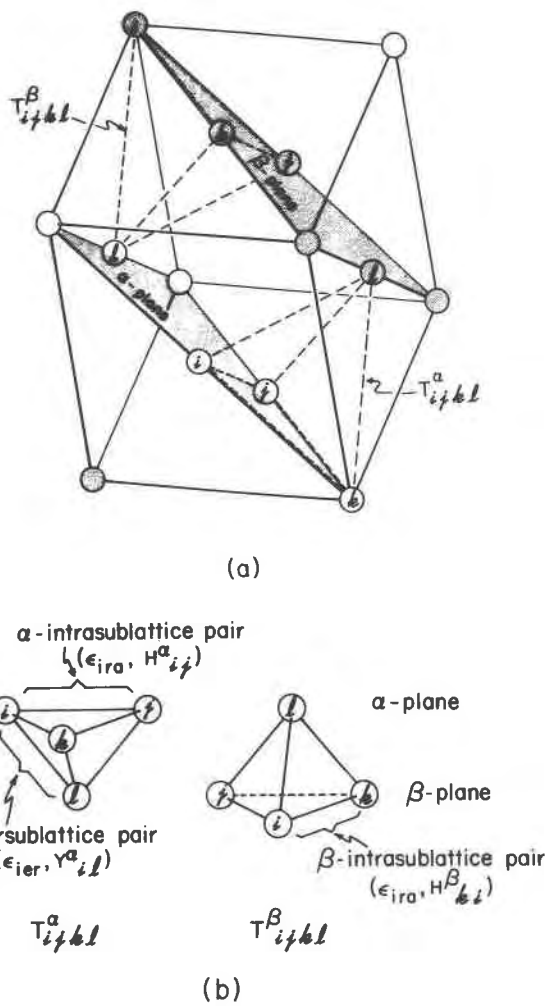

Fig. 2. (a) Schematic drawing of a trigonally distorted fcc lattice with alternating α and β planes. (b) Tetrahedron basic clusters corresponding to the distribution variables T^{α}_{ijkl} and T^{β}_{ijkl}; also indicating the energy parameters and subcluster distribution variables associated with intersublattice (ε_{ier}, Y^{α}_{il}) and intrasublattice (ε_{ira}, H^{α}_{ij}) near neighbor pairs.

we ignore other possible contributions to the configurational entropy, such as rotational disordering of CO_3 groups, and consider only the contribution from cation disordering, we may treat $CaCO_3$–$MgCO_3$ as if it were a binary fcc-derived alloy in which metal atoms are replaced by corner- and edge-sharing M–O_6 octahedra.

In a CVM calculation the free energy of solution (deviation from mechanical mixing) is expressed as a function of distribution variables and configurational internal energies for some small basic cluster of atoms. Basic cluster distribution variables indicate the probability of finding the basic cluster in some specified configuration, and an independent subset of these variables contains all the thermodynamic information available in the approximation. The CVM forms a hierarchical set of approximations in which a basic cluster of a single site is equivalent to the Bragg-Williams approximation; a pair of sites as basic cluster is equivalent to Bethe's approximation and, in general, a larger basic cluster gives a better approximation (Kikuchi, 1951). For this calculation we take a tetrahedron as the basic cluster because it is the simplest three-dimensional figure which allows us to consider both intersublattice- and intrasublattice-pair correlations. As our results show, intersublattice interactions are associated with ordering and intrasublattice interactions with exsolution. Thus, an explicit link is established between specific categories of interactions and specific features of the phase diagrams.

The grand potential

The thermodynamic function we minimize is called the grand potential and is defined as:

$$\hat{g} \equiv E - TS - \sum_i \mu_i N_i \qquad i = 1, 2 \tag{1}$$

where $\hat{g}$ is the grand potential, E is the internal energy of solution, T is absolute temperature, S is configurational entropy, μ_i is the chemical potential of species-i and N_i is the number of species-i atoms in the system.

The grand potential for an N-site system in the dolomite structure ordered phase can be expressed (in a normalized form) as:

$$\phi_{ord} \equiv \phi_\alpha + \phi_\beta \equiv \hat{g}/NnT, \tag{2a}$$

where k is Boltzmann's constant and (from the derivation in Appendix I)

$$\phi_\alpha = \beta\{\varepsilon_{ijkl} - \tfrac{1}{8}(\mu_i + \mu_j + \mu_k + \mu_l)\}T^\alpha_{ijkl}$$
$$+ \sum_{ijkl} L(T^\alpha_{ijkl}) - \frac{1}{2}\left[\sum_{ij} L(H^\alpha_{ij}) + \sum_{jk} L(H^\alpha_{jk}) + \sum_{ki} L(H^\alpha_{ki})\right]$$
$$- \frac{1}{2}\left[\sum_{il} L(Y^\alpha_{il}) + \sum_{jl} L(Y^\alpha_{jl}) + \sum_{kl} L(Y^\alpha_{kl})\right] \tag{2b}$$
$$+ \frac{5}{8}\left[\sum_i L(X^\alpha_i) + \sum_j L(X^\alpha_j) + \sum_k L(X^\alpha_k) + \sum_l L(X^\beta_l)\right]$$
$$+ \beta\lambda_\alpha\left(1 - \sum_{ijkl} T^\alpha_{ijkl}\right) + \sum_{ijkl} (\alpha_{il} + \alpha_{jl} + \alpha_{kl})T^\alpha_{ijkl}$$

and

$$\phi_\beta = \beta\{\varepsilon_{ijkl} - \tfrac{1}{8}(\mu_i + \mu_j + \mu_k + \mu_l)\}T^\beta_{ijkl}$$
$$+ \sum_{ijkl} L(T^\beta_{ijkl}) - \frac{1}{2}\left[\sum_{ij} L(H^\beta_{ij}) + \sum_{jk} L(H^\beta_{jk}) + \sum_{ki} L(H^\beta_{ki})\right]$$
$$- \frac{1}{2}\left[\sum_{li} L(Y^\beta_{li}) + \sum_{lj} L(Y^\beta_{lj}) + \sum_{lk} L(Y^\beta_{lk})\right] \tag{2c}$$
$$+ \frac{5}{8}\left[\sum_i L(X^\beta_i) + \sum_j L(X^\beta_j) + \sum_k L(X^\beta_k) + \sum_l L(X^\alpha_l)\right]$$
$$+ \beta\lambda_\beta\left(1 - \sum_{ijkl} T^\beta_{ijkl}\right) - \sum_{ijkl} (\alpha_{li} + \alpha_{lj} + \alpha_{lk})T^\beta_{ijkl}.$$

Here i,j,k,l = 1,2; $L(x) \equiv x \ln x - x$; T^α_{ijkl}, Y^α_{il}, H^α_{ij} and X^α_i are distribution variables for T^α tetrahedra, Y^α intersublattice pairs, H^α intrasublattice pairs, and X^α sites, respectively (and similarly for β variables; Fig. 2b); $\beta \equiv (kT)^{-1}$; ϵ_{ijkl} is the internal energy of solution of a tetrahedron in configuration ijkl; and the terms λ_α λ_β, α_{il}, α_{jl}, α_{kl} are Lagrange multipliers which constrain T variables to be normalized and to have appropriate symmetry (Appendix I). The normalized grand potential for the disordered phase (ϕ_{dis}) can be obtained from equation (2) by including the additional constraint $T^\alpha_{ijkl} = T^\beta_{ijkl}$.

If we take the indices 1 and 2 to signify Ca^{++} and Mg^{++}, respectively, then for example, T^α_{1112} indicates the probability of finding a tetrahedron with three Ca^{++} on sublattice-α and one Mg^{++} on sublattice-β. The Y's, H's, and X's are called subcluster distribution variables and describe the probabilities of finding certain short-range correlations in the system. Subcluster variables may be regarded as dependent variables because they are related to the basic cluster variables by geometrical equations of the form:

$$Y_{il} = Y^\alpha_{il} = Y^\beta_{il} = \sum_{jk} T^\alpha_{ijkl} = \sum_{jk} T^\beta_{ijki} \tag{3a}$$

$$H^\alpha_{ij} = \sum_{kl} T^\alpha_{ijkl} \tag{3b}$$

$$X^\alpha_i = \sum_{jkl} T^\alpha_{ijkl} = \sum_{jkl} T^\beta_{jkli} \tag{3c}$$

where the summation is always taken over those indices not appearing in the subcluster variable of interest. Equation (3a), for example, expresses the probability of finding a Y-type pair with species-i on sublattice α and species-l on sublattice β; Eq. (3b) gives the probability of finding an i–j pair with both atoms on sublattice-α and Equation (3c) gives the probability of finding species-i on sublattice α Similar equations may be written for H^{β} pairs and triangles.

Minimizing equations (2b) and (2c) with respect to T^{α}_{ijkl} and T^{β}_{ijkl}, respectively (at fixed T and μ), and solving the resultants for T^{α}_{ijkl} and T^{β}_{ijkl} yields:

$$\ln T^{\alpha}_{ijkl} = \beta[\tfrac{1}{8}(\mu_i + \mu_j + \mu_k + \mu_l) - \varepsilon_{ijkl}] + \beta\lambda_{\alpha} + \alpha_{il} + \alpha_{jl} + \alpha_{kl} + \ln \frac{(H^{\alpha}_{ij}H^{\alpha}_{jk}H^{\alpha}_{ki}Y^{\alpha}_{il}Y^{\alpha}_{jl}Y^{\alpha}_{kl})^{1/2}}{(X^{\alpha}_{i}X^{\alpha}_{j}X^{\alpha}_{k}X^{\beta}_{l})^{5/8}} \tag{4a}$$

$$\ln T^{\beta}_{ijkl} = \beta[\tfrac{1}{8}(\mu_i + \mu_j + \mu_k + \mu_l) - \varepsilon_{ijkl}] + \beta\lambda_{\beta} - \alpha_{li} - \alpha_{lj} - \alpha_{lk} + \ln \frac{(H^{\beta}_{ij}H^{\beta}_{jk}H^{\beta}_{ki}Y^{\beta}_{il}Y^{\beta}_{jl}Y^{\beta}_{kl})^{1/2}}{(X^{\beta}_{i}X^{\beta}_{j}X^{\beta}_{k}X^{\alpha}_{l})^{5/8}} \tag{4b}$$

Note that in differentiating (2b) and (2c) we treat T variables as independent, and maintain a strict separation of α- and β-variables throughout (*e.g.*, Y^{α}_{il} and Y^{β}_{il} are numerically equal but when we differentiate, we treat Y^{α}_{il} as a function of T^{α}_{ijkl} only and Y^{β}_{il} as a function of T^{β}_{ijkl} only). Equations (4a) and (4b) can be solved numerically for T^{α}_{ijkl} and T^{β}_{ijkl} by a combination of the Natural Iteration Method (Kikuchi, 1974) and the Minor Iteration Technique (Kikuchi, 1976). An alternate method for solving equations of this type, based on a Newton-Raphson approach, is given by Sanchez and deFontaine (1979).

Coexisting phases

With the Natural Iteration Method the calculation is done at fixed values of T and μ to obtain equilibrium values for the distribution variables. The bulk composition and other quantities such as S_{LRO} and various SRO parameters, may then be calculated with the geometrical equations. Compositions of coexisting ordered and disordered phases are determined by locating the intersection of ϕ_{ord} *vs.* μ and ϕ_{dis} *vs.* μ at fixed temperature. In practice, the ϕ *vs.* μ curves are almost linear, and we find the two-phase equilibrium value for μ by an iterative technique based on linear extrapolation.

Tricritical points

Close to a tricritical point it is very difficult to calculate the compositions of coexisting phases with any precision. This unfortunate situation occurs because the curves Φ_{ord} *vs.* μ and Φ_{dis} *vs.* μ have identical slopes at a tricritical point and, therefore, relatively large changes in μ (and, therefore, X) produce relatively small differences in energy between the ordered and disordered phases ($\Phi_{ord} - \Phi_{dis}$). For this reason we do not have great confidence in our estimated values for $\{X_3,T_3\}$ and $\{X_3',T_3'\}$, and we are somewhat unsure about the shape of our calculated diagrams in this region. A related problem is that the Natural Iteration Method calculation converges very slowly near a tricritical point, again because of the small difference in energy between the ordered and disordered phases. This situation is analogous to the experimental problem of obtaining an equilibrium assemblage when energy differences are small.

Second-order transition

The second-order transition curve, corresponding to λ in Figure 1, is obtained by evaluating the determinant of a Hessian matrix [H]:

$$\det[H] = \det[\partial^2\Phi_{ord}/\partial v_m \partial v_n]_{dis} = 0 \qquad m,n = 1,2, \ldots 5$$

where the subscripts (ord and dis) indicate that differentiations are performed on Φ_{ord} but the numerical calculation is performed for Φ_{dis}. The v variables are a set of five independent parameters which define the LRO:

$$v_1 \equiv \Delta_{1121} \tag{6a}$$

$$v_2 \equiv \Delta_{2211} \tag{6b}$$

$$v_3 \equiv (1/2)(\Delta_{2221} - \Delta_{1112}) \tag{6c}$$

$$v_4 \equiv \Delta_{1122} \tag{6d}$$

$$v_5 \equiv \Delta_{2212} \tag{6e}$$

where $\Delta_{ijkl} \equiv 1/2(T^{\alpha}_{ijkl} - T^{\beta}_{ijkl})$ and linear constraints of normalization and symmetry require four dependent u-variables;

$$u_1 \equiv \Delta_{1111} = -2v_1 - v_2 \tag{7a}$$

$$u_2 \equiv \Delta_{2221} = -v_1/2 - v_2 + v_3 - v_4 - v_5/2 \tag{7b}$$

$$u_3 \equiv \Delta_{1112} = -v_1/2 - v_2 - v_3 - v_4 - v_5/2 \tag{7c}$$

$$u_4 \equiv \Delta_{2222} = -2v_5 - v_4 \tag{7d}$$

Note that at the composition $X = 0.5$, for a perfectly symmetrical phase diagram, we have accidental degeneracies such that $v_1 = v_5$, and $v_2 = v_4$; thus, we have chosen the v-variables in a way that maximizes the symmetry of [H].

With the above definition for the Hessian, det[H] is a discriminatory function such that: det[H] = 0 defines T_c; det[H] > 0 characterizes the disordered region; and det[H] < 0 characterizes the ordered region. Because the sign of det[H] changes across the transition, it is easy to set up an iterative calculation which converges toward T_c. All values used in constructing the theoretical diagrams presented in this paper are converged such that $T^{+} - T^{-} < 0.00001$, where $T^{-} < T_c < T^{+}$; and superscripts (+ and −) indicate the sign of det[H] at these temperatures.

Energy parameters

Calculated phase relations depend critically upon the signs and magnitudes of energy parameters. As a first approximation, we write the tetrahedron energy as a sum of intersublattice- and intrasublattice-pseudopairwise energy parameters, ε_{ier} and ε_{ira}, respectively. Here, the intersublattice nn-pairs are i–l, j–l, k–l, and the intrasublattice nn-pairs are i–j, j–k, k–i (Fig. 2b); and we use the term pseudopairwise to emphasize that these need not be two atom interactions, but may just as reasonably be regarded as interactions between corner- and edge-sharing $M–O_6$ octahedra. In general, negative parameters stabilize 1–2 nn-pairs and are associated with ordering, while positive parameters destabilize 1–2 nn-pairs and are associated with exsolution. The parameter ε_{ier} is defined in the usual way as:

$$\varepsilon_{ier} = \varepsilon_{12,ier} - (1/2)(\varepsilon_{11,ier} + \varepsilon_{22,ier}) \tag{8a}$$

and similarly for ε_{ira}, such that

$$\varepsilon_{ijkl} = (1/2)(n_{ijkl}\varepsilon_{ier} + m_{ijkl}\varepsilon_{ira}) \tag{8b}$$

where the factor 1/2 is included because each pair is shared by two tetrahedra; n_{ijkl} is the number of 1–2 intersublattice nn-pairs; and m_{ijkl} is the number of 1–2 intrasublattice nn-pairs in configuration ijkl.

Constraints on ε_{ier} and ε_{ira}

For the dolomite structure phase to be stable, and the calculated phase diagram to resemble Figure 1, three constraints must apply to the energy parameters:

(1) $\varepsilon_{ier} < 0$
(2) $\varepsilon_{ier} < 2e_{ira}$
(3) $\varepsilon_{ira} > 0$

Constraint (1) simply expresses the necessity of assigning negative energies to configurations which characterize the dolomite structure ordered phase (configurations associated with the variables T^{α}_{1112} and T^{β}_{2221}), such that

$$\varepsilon_{1112} = \varepsilon_{2221} = (3/2)\varepsilon_{ier} < 0. \tag{9}$$

Constraint (2) applies because configurations with two atoms of each species (*e.g.*, 1122, 1212, . . . , *etc.*) have energies

$$\varepsilon_{1122} = \varepsilon_{1212} = \ldots = \varepsilon_{ier} + \varepsilon_{ira} \tag{10}$$

Thus, if constraint (2) is violated, then an ordering scheme based on these configurations will be lower in energy than the dolomite structure scheme.

Constraint (3) is less obvious than (1) or (2). We find that for $\varepsilon_{ira} < 0$ the dolomite structure-calcite structure transition is first-order in character (as for AB-type ordering in the Cu–Au system; Van Baal, 1973; Kikuchi, 1974) and the calculated phase diagram resembles the Cu–Au diagram, neglecting those features related to A_3B-, and AB_3-type ordering. That is, the calculation predicts a diagram in which narrow two-phase fields (joined at a point at or near $X = 0.5$) separate the ordered and disordered regions, and the line defined by det[H] = 0 occurs metastably, below the transition temperature. The reason for this result (Kikuchi and Sato, 1974) is that favorable 1–2 intrasublattice configurations compete with more favorable 1–2 intersublattice configurations, suppressing the transition temperature, and imposing some first-order character on the transition.

Results of these calculations and others (Burton, 1982) support an interesting generalization concerning the relationship between energy parameters and phase diagrams predicted by CVM approximations:

(a) When the sum of intersublattice interactions is negative and the sum of intrasublattice interactions is also negative, then the transition is first-order as in the Cu–Au system.

(b) However, when the sum of intersublattice interactions is negative but the sum of intrasublattice interactions is positive, then the transition is second-order above T_3 and first-order below, as in Figure 1.

It should be noted that CVM calculations are by no means tied to a pairwise interpretation for the energy parameters, and that we use this approach only as a convenience. Any method which provides a set of tetrahedron energies would serve as well, and the above stated generalization would still apply. We note, however, that for more complicated nonconvergent systems the statements above may require some modification.

Comparison with Experiment I (Quantitative Constraints)

Stabilization energy of dolomite $X = 0.5$

We have shown above that certain *a priori* constraints apply to ε_{ier} and ε_{ira}, if we are to calculate a diagram with the appropriate topology and we now consider some more quantitative constraints provided by experimental studies:

(1′) 1100°C $< T_c <$ 1150°C at $X = 0.5$ (Reeder and Nakajima, 1982).

(2′)[3] $\Delta H^{\circ}_{dol} = -3.8(\pm 1.1)$ kJ/mole (calculated from data for the enthalpy of formation from oxides; in Robie *et al.*, 1979) where $\Delta H^{\circ}_{dol} \equiv H^{\circ}_{dolomite} - H^{\circ}_{calcite} - H^{\circ}_{magnesite}$.

(3′) $\{X_3, T_3\} \approx \{0.42, 1070°C\}$ (from the experimental diagram of Goldsmith and Heard, 1961).

Given our very simplified and inflexible formulation for the internal energy and the approximate nature of the

[3] Note that this value of ΔH°_{dol} is rather modest but the critical temperature is quite high. These apparently contradictory observations provide another rationale for the assignment $\varepsilon_{ira} > 0$: repulsive intrasublattice interactions imply resistance to disordering and therefore a high value for T_c.

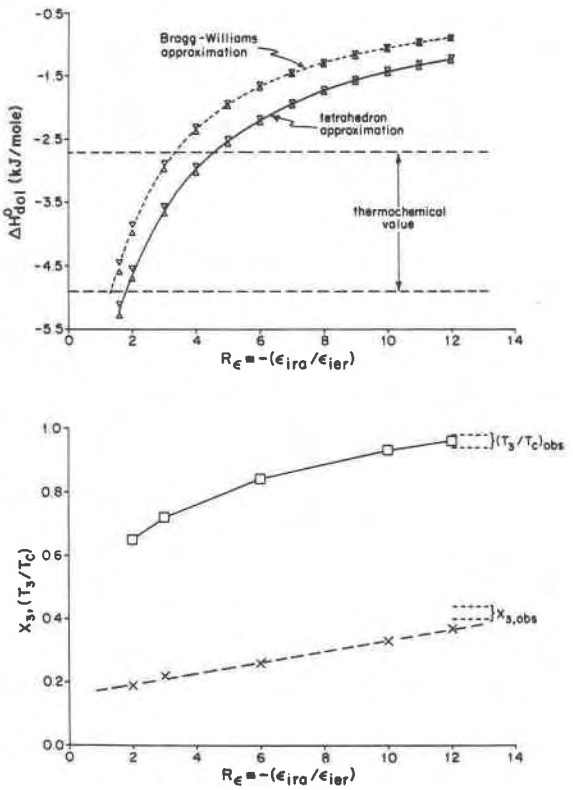

Fig. 3. (a) The enthalpy of stabilization of dolomite, ΔH°_{dol}, as a function of R_ε ($R_\varepsilon \equiv -\varepsilon_{ira}/\varepsilon_{ier}$). The horizontal dashed lines indicate the thermochemical value ($\Delta H^{\circ}_{dol} = 3.8 \pm 1.1$ kJ/mole from Robie *et al.*, 1979); the solid curve gives calculated values for the tetrahedron approximation; and the dashed curve gives calculated values for the Bragg–Williams approximation. Note that for a fixed value of T_c, the tetrahedron approximation always gives a lower value for ΔH°_{dol} than the Bragg–Williams approximation. (b) The quantities (T_3/T_c) and X_3 as functions of R_ε. Note that a value of $R_\varepsilon \gtrsim 12$ is required for agreement with the experimental diagram, as opposed to the value $2 \lesssim R_\varepsilon \lesssim 4.5$ that is indicated by Fig. 3a.

treatment as a whole, we do not expect to satisfy all three constraints simultaneously, and indeed this is not possible. It is an instructive exercise, however, to calculate ΔH°_{dol} (constraint 2′) from the experimental brackets for T_c (constraint 1′) and compare the results with a Bragg–Williams approximation.

In Figure 3a we plot ΔH°_{dol} as a function of the parameter R_ε where

$$R_\varepsilon \equiv -(\varepsilon_{ira}/\varepsilon_{ier}) \tag{11}$$

The horizontal dashed lines in Figure 3a indicate the thermochemical value for ΔH°_{dol} (constraint 2′); the solid curve is for the tetrahedron-approximation; and the dashed curve gives the Bragg–Williams approximation. We expect both approximations to overestimate the configurational entropy and, therefore, to underestimate the stabilization energy (*i.e.*, $\Delta H^{\circ}_{calc} > \Delta H^{\circ}_{obs}$). Thus, the lower value of ΔH°_{dol} that is obtained in the tetrahedron-approximation (for all values of R_ε) should be interpreted as indicating improved agreement with the experimental data.

To obtain the tetrahedron-approximation curve we calculate τ_c (temperature in reduced units) as a function of R_ε where

$$\tau_c = -2kT_c/3\varepsilon_{ier} \tag{12a}$$

and make the approximations

$$3\varepsilon_{ier} \approx \Delta E^{\circ}_{dol} \approx \Delta H^{\circ}_{dol} \tag{12b}$$

In the corresponding Bragg–Williams case we have

$$Z_{ier}\varepsilon_{ier} - Z_{ira}\varepsilon_{ira} = -2kT_c \tag{13a}$$

or

$$3\varepsilon_{ier} = -2kT_c/(Z_{ier} + Z_{ira}R_\varepsilon) \tag{13b}$$

where Z_{ier} and Z_{ira} are coordination numbers for inter- and intrasublattice cation-cation nn-pairs, respectively, and in this case $Z_{ier} = Z_{ira} = 6$.

In Figure 3b we plot the parameters (T_3/T_c) and X_3 as functions of R_ε and compare them with the corresponding experimental data (constraint 3′). Our plotted values for T_3/T_c) and X_3 have been estimated graphically and, as indicated above, are subject to some uncertainty. Nonetheless, Figure 3b indicates that a value of $R_\varepsilon \gtrsim 12$ is required and this result clearly contradicts constraint 2′ and Figure 3a, which suggest $2 \lesssim R_\varepsilon \lesssim 4.5$.

Importance of SRO

Improved agreement in the tetrahedron case (a more negative value for ΔH°_{dol}) is a direct consequence of including SRO in the theory. The tetrahedron calculation predicts a second-order transition with substantial SRO above T_c (Figure 4), and, therefore, a λ-type specific heat curve ($C_v(T)$) with a significant high-temperature tail (note that here $C_v(T)$ is only the configurational contribution to the specific heat). The Bragg–Williams approximation assumes no SRO above T_c, and, therefore, no high-temperature tail. In Figure 4 we plot S_{LRO}, $\sigma_{12,ier} \equiv Y_{12} + Y_{21}$ and $\sigma_{12,ira} \equiv H^{\alpha}_{12} + H^{\alpha}_{21}$ as functions of reduced temperature (T/T_c). Above $T/T_c = 1$, the Bragg–Williams approximation assumes that both $\sigma_{12,ier}$ and $\sigma_{12,ira}$ have the random distribution value of 0.5 (horizontal dashed line), however, the tetrahedron-approximation predicts a small, but significant, positive deviation (from 0.5) for $\sigma_{12,ier}$ and a very large negative deviation for $\sigma_{12,ira}$. Note that the relative magnitudes of these deviations are similar to the relative absolute magnitudes of ε_{ier} and ε_{ira} as one would expect.

Analytically, the relationship between ΔE°_{dol}, $C_v(T)$, and SRO can be understood by considering the energy of transition (ΔE_{trans}) from the completely ordered state (with energy $E_{T=0}$) to the completely disordered state (with energy $E_{T=\infty}$).

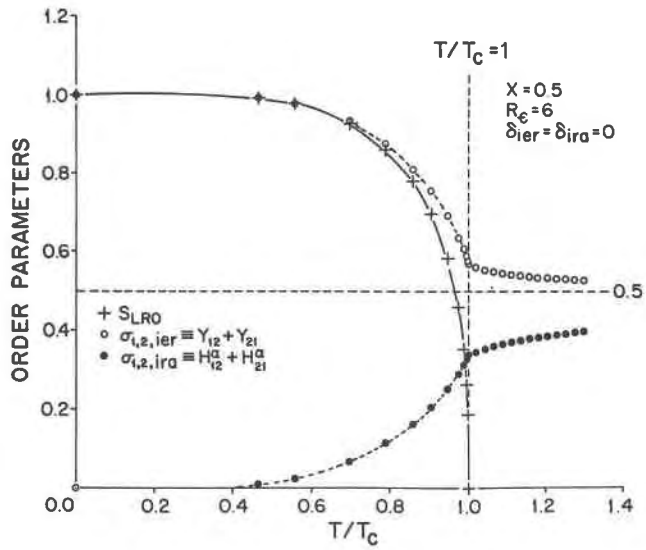

Fig. 4. The long-range order parameter (S_{LRO} = crosses), and two short-range order parameters, $\sigma_{12,ier} \equiv Y_{12} + Y_{21}$ (open circles) and $\sigma_{12,ira} \equiv H^{\alpha}_{12} + H^{\alpha}_{21}$ (closed circles), as functions of reduced temperature (T/T_c) for $X = 0.5$ and $R_\varepsilon = 6$. Note that above $T/T_c = 1$ both SRO parameters deviate significantly from the random distribution value of 0.5; also note that $\sigma_{12,ier}$ deviates far less than $\sigma_{12,ira}$ because the absolute value of ε_{ier} is a factor of six smaller than the absolute value of ε_{ira}.

$$E_{T=0} = 3\varepsilon_{ier} \approx \Delta E^{\circ}_{dol} \tag{14a}$$

$$E_{T=\infty} = (3/2)(\varepsilon_{ier} + \varepsilon_{ira}) \tag{14b}$$

$$\Delta E_{trans} \equiv E_{T=\infty} - E_{T=0} = \int_0^{\infty} C_v dT \tag{14c}$$

Substituting $-R_\varepsilon\varepsilon_{ier} = \varepsilon_{ira}$, separating the integral into low- and high-temperature parts, and solving for ΔE°_{dol} we obtain

$$\Delta E^{\circ}_{dol} \approx -\left(\frac{2}{R_\varepsilon + 1}\right)\left[\int_0^{T_c} C_v dT + \int_{T_c}^{\infty} C_v dT\right] \tag{15}$$

The first integral in Equation (15) gives the energy associated with loss of LRO and low-temperature SRO in the system. The second gives the energy required to remove SRO above T_c, and it is this residual configurational energy above T_c (included in the tetrahedron case but assumed to be zero in the Bragg–Williams case) which accounts for the more negative ΔH°_{dol} calculated in the tetrahedron-approximation.

Comparison with experiment II (phase diagrams)

Phase diagram symmetry

Figure 5 (solid curve) is the calculated phase diagram for $R_\varepsilon = 2$. This diagram is symmetric about the composition $X = 0.5$ because we have made ε_{ijkl} a function of pairwise parameters that are independent of composition. To obtain an asymmetric diagram, one must either include composition dependence in the energy parameters, or use many-body interactions as done by Van Baal (1973). In the Natural Iteration Method based on the grand potential, it is easier to use composition independent parameters because the calculation is done with fixed μ rather than fixed X; and, therefore, we have adopted the many-body approach (Figure 5, dashed curve). The specific parameters we add are called δ_{ier} and δ_{ira}, and we simply append the factor $(N_{2,ijkl} - 2)\delta_{ier}$ to ε_{ier} and likewise for ε_{ira} such that

$$\varepsilon_{ijkl} = (1/2)\{n_{ijkl}[\varepsilon_{ier} + (N_{2,ijkl} - 2)\delta_{ier}] + m_{ijkl}[\varepsilon_{ira} + (N_{2,ijkl} - 2)\delta_{ira}]\} \tag{16}$$

where $N_{2,ijkl}$ is the number of species-2 (Mg) atoms in configuration ijkl; and the many-body parameters δ_{ier} and δ_{ira} are treated as perturbations on ε_{ier} and ε_{ira}, respectively. Although it is possible to produce an asymmetric phase diagram with only one such parameter, it seems more reasonable to treat many-body perturbations of ε_{ier} and ε_{ira} as independent. In Figure 5 we take both δ_{ier} and δ_{ira} to be positive which has the effect of stabilizing configurations with three species-1 (Ca) atoms and destabilizing configurations with three species-2 (Mg) atoms. Physically, the assignments $\delta_{ier} > 0$ and $\delta_{ira} > 0$ can be rationalized in terms of the empirical crystal chemical generalization that it requires more energy to put an oversized ion in an undersized site than vice versa: *i.e.*, configurations with three Mg atoms are regarded as Mg-rich environments characterized by relatively small sites and configurations with three Ca atoms are regarded as Mg-poor environments characterized by relatively large sites (We note that this rationale makes more sense for δ_{ira} than for δ_{ier}, because intrasublattice interactions involve edge sharing $M–O_6$ octahedra whereas intersub-

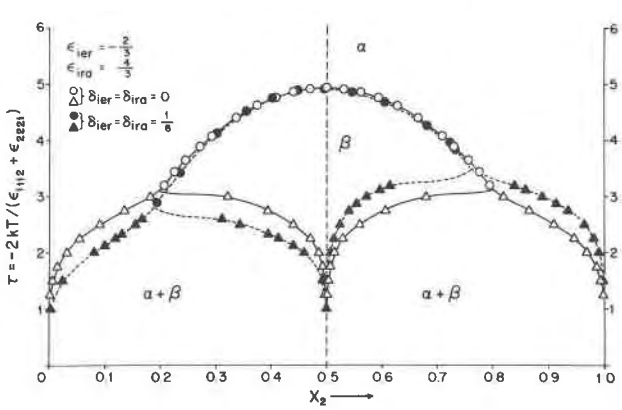

Fig. 5. The solid line (with open symbols) indicates the symmetric diagram calculated with $R_\varepsilon = 2$ and $\delta_{ier} = \delta_{ira} = 0$. The dashed line (with closed symbols) gives the asymmetric diagram for $R_\varepsilon = 2$, $\delta_{ier} = \delta_{ira} = -\varepsilon_{ier}/4$. Note the effect of δ_{ier} and δ_{ira} on T_3 and T_3'.

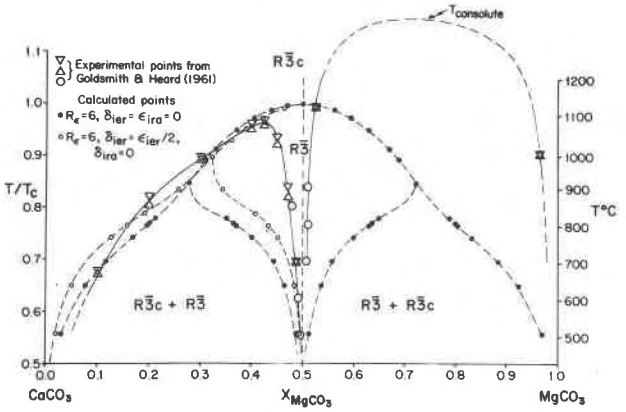

Fig. 6. Comparison of calculated diagrams with the experimental diagram of Goldsmith and Heard (1961). The experimental diagram is given by the solid line through open symbols. The dashed curve through closed dots gives the tetrahedron approximation for $R_\varepsilon = 6$ and $\delta_{ier} = \delta_{ira} = 0$. The dashed line through open dots is the tetrahedron approximation for $R_\varepsilon = 6$, $\delta_{ier} = \varepsilon_{ier}/2$, and $\delta_{ira} = 0$. Note that we have taken $T_c = 1125$°C and that the projected value for $T_{consolute}$ is far above T_c.

lattice interactions are between corner sharing octahedra.) In Figure 5 (dashed curve) we plot our calculated diagram for $\varepsilon_{ier} = -2/3$, $\varepsilon_{ira} = 4/3$, and $\delta_{ier} = \delta_{ira} = 1/6$ (in reduced units). Note that the resulting asymmetry is in qualitative agreement with the experimental diagram, with respect to the inequality $T_3 < T_3'$.

Calcite-dolomite $0 < X < 0.5$

In Figure 6 we compare our calculated diagrams for $R_\varepsilon = 6$, $\delta_{ier} = \delta_{ira} = 0$ and $R_\varepsilon = 6$, $\delta_{ier} = \varepsilon_{ier}/2$ and $\delta_{ira} = 0.0$ (in reduced units) with the experimental diagram of Goldsmith and Heard (1961). We regard the calculated diagram as being in qualitative to semi-quantitative agreement with the experimental one and find that including δ_{ier} improves this agreement somewhat. We note, however, that such a large value of δ_{ier} ($\delta_{ier} = \varepsilon_{ier}/2$) seems rather artificial. It should also be noted that we achieve a level of quantitative agreement which is comparable to, or better than, the Navrotsky and Loucks (1977) calculation; however, we generate the full asymmetric diagram with only three energy parameters (as opposed to four), and we calculate many more order parameters. We regard the reduction in energy parameters as unimportant here because it is also possible to construct an asymmetric Bragg–Williams approximation with only three parameters; however, the calculation of SRO parameters clearly distinguishes the tetrahedron-approximation as a more complete and physically rigorous theoretical treatment than the Navrotsky and Loucks model.

A smaller value for R_ε gives improved agreement for ΔH°_{dol} but worse agreement for $\{X_3, T_3\}$; so that we regard the value of $R_\varepsilon = 6$ as a reasonable compromise. Quantitative agreement could be improved by including composition and/or temperature dependence in R_ε but if, for example, we include only composition dependence, then R_ε must decrease by a factor of three to four between $X = 0.5$ and $X = 0.4$ which is quite dramatic. An alternative approach would be to use a larger cluster approximation, implying a lower ΔH°_{dol}, and include a greater number of many-body parameters.

Dolomite–magnesite $0.5 < X < 1$

In all calculated diagrams $T_{consolute} = T_3' < T_c$, in conflict with experimental results for the Mg-rich side of the diagram. This occurs because we consider only the transition involving formation of the dolomite-structure ordered phase and therefore generate only one minimum in $\Phi_{soln}(T, \mu, T_{1111}, T_{1112}, \ldots)$. Thus, we have only one λ-curve, the metastable extensions of which must become ordering spinodals below T_3 and T_3' (Fig. 1). Since spinodal curves must pass through $T_{consolute}$, and since we have only one such curve associated with instability of the disordered phase, the calculated value of $T_{consolute}$ must lie on the curve λ and must, therefore, equal T_3'. In order to relax this restriction, we require another configurational degree of freedom—such as a third component or another ordering possibility.

Our speculations on possible sources for another degree of freedom center on the CO_3 groups, as they are the structural element we ignored in formulating the model. Slight decarbonation of Mg-rich solutions leading to a defect structure in which, for example, an $O^=$ ion replaces a CO_3 group would provide a third component. We know of no experimental evidence to suggest this, but stoichiometry could, at least in principle, be tested by quantitative analysis. A more likely explanation is that another phase transition occurs, in which CO_3 groups become orientationally disordered at high temperatures. A transition of this type has been shown to occur in $NaNO_3$, which is structurally analogous to $CaCO_3$ (Rao *et al.*, 1975; Paul and Pryor, 1971); and it has been suggested (Mirwald, 1979; Salje and Viswanathan, 1976) that the $CaCO_3$-I to $CaCO_3$-IV transition is also of this type. Thus, it seems plausible that a similar transition might occur in Mg-rich solutions. The CO_3 groups may be regarded as occupying all octahedral interstices in the distorted-fcc cation lattice; and, thus, to include CO_3 group orientation in the model would require at least a tetrahedron–octahedron approximation, which implies, nominally, 2^8 basic cluster variables as opposed to 2^4 for the tetrahedron-approximation. Note that the octahedron approximation, which would seem the most natural choice, fails to converge to the ordered phase (Kurata *et al.*, 1953).

Conclusions

Our results support the general conclusion that phase diagrams resembling Figure 1 occur when the sum of intersublattice interaction parameters is negative but the

sum of intrasublattice parameters is positive, at least for convergent ordering systems. With $R_\varepsilon = 6$, we achieve semiquantitative agreement with thermochemical data for the stabilization energy of dolomite, ΔH°_{dol} and demonstrate that including SRO in the theory improves agreement for this quantity relative to a Bragg–Williams approximation. The tetrahedron-approximation predicts substantial SRO in disordered dolomites (above T_c) and therefore a λ-type specific heat curve with a significant high-temperature tail. We obtain qualitative to semiquantitative agreement between theoretical and experimental diagrams for the segment $0 < X < 0.5$ and find that including the many-body parameter δ_{ier} improves the agreement somewhat. We suggest that including composition and/or temperature dependence in R_ε would produce better quantitative results but note that rather dramatic dependence is required to achieve full quanitative agreement.

For the segment $0.5 < X < 1$ we fail to achieve even qualitative agreement with experiment, with respect to the relative positions of T_3' and $T_{consolute}$; and we note that this inadequacy of our model could be remedied by including either another component or another phase transition. We speculate that a transition based on rotational disordering of CO_3 groups might provide the additional degree of freedom we require.

Acknowledgments

This research was supported by NSF grant No. EAR8025260 and NASA grant No. NGL33-015-130. The first author gratefully acknowledges the helpful comments and criticism of D. H. Lindsley and P. M. Davidson.

References

Allen, S. A. and Cahn, J. W. (1976) On tricritical points resulting from the intersection of higher-order transitions with spinodals. Scripta Metallurgica, 10, 451–454.

Althoff, P. L. (1977) Structural refinements of dolomite and a magnesian calcite and implications for dolomite formation in the marine environment. American Mineralogist, 62, 722–783.

Barker, J. A. (1953) Methods of approximation in the theory of regular mixtures. Proceedings of the Royal Society (London), A216, 45–56.

Burton, B. P. (1982) Thermodynamic analysis of the systems $CaCO_3$–$MgCO_3$, α-FE_2O_3, and Fe_2O_3–$FeTiO_3$. Ph.D. Thesis, State University of New York at Stony Brook.

Burton, B. P. and Kikuchi, R. (1981) Cluster-variation method models of phase relations in the systems Fe_2O_3-$FeTiO_3$ and $CaCO_3$–$MgCO_3$. (abstr.) Geological Society of America Abstracts with Programs, 13, 420.

Byrnes, A. P. and Wyllie, P. J. (1981) Subsolidus and melting relations for the join $CaCO_3$–$MgCO_3$ at 10 kbar. Geochimica et Cosmochimica Acta, 45, 321–328.

Carpenter, M. A. (1978) Kinetic control of ordering and exsolution in omphacite. Contributions to Mineralogy and Petrology, 67, 17–24.

Carpenter, M. A. (1981) A "conditional spinodal" within the peristerite miscibility gap of plagioclase feldspar. American Mineralogist, 66, 553–560.

Goldsmith, J. R. (1972) Cadmium dolomite and the system $CdCO_3$–$MgCO_3$, Journal of Geology, 80, 611–626.

Goldsmith, J. R. and Newton, R. C. (1969) P–T–X relations in the system $CaCO_3$–$MgCO_3$ at high temperatures and pressures, American Journal of Science, 267-A, 160–190.

Goldsmith, J. R. and Heard, H. C. (1961) Subsolidus phase relations in the system $CaCO_3$–$MgCO_3$. Journal of Geology, 69, 453–457.

Irving, A. J. and Wyllie, P. J. (1975) Subsolidus and melting relationships for calcite, magnesite and the join $CaCO_3$–$MgCO_3$ to 36 kb. Geochimica et Cosmochimica Acta, 39, 35–53.

Kikuchi, R. (1951) A theory of cooperative phenomena. The Physical Review, 81, 988–1003.

Kikuchi, R. (1974) Superposition approximation and natural iteration calculation in cluster-variation method. Journal of Chemical Physics, 60, 1071–1080.

Kikuchi, R. (1976) Natural iteration method and boundary free energy. Journal of Chemical Physics, 65, 4545–4553.

Kikuchi, R. and Sato, H. (1974) Characteristics of superlattice formation in alloys of face-centered cubic structure. Acta Metallurgica, 22, 1099–1112.

Kurata, M., Kikuchi, R., and Watari, T. (1953) A theory of cooperative phenomena. III. Detailed discussions of the cluster variation method. Journal of Chemical Physics, 21, 434–447.

Merkel, G. A. and Blencoe, J. G. (1982) Thermodynamic procedures for treating the monoclinic/triclinic inversion as a high-order phase transition in equations of state for binary analbite-sanidine feldspars. In Advances in Physical Geochemistry, 2, 244–284. Springer-Verlag, New York.

Mirwald, P. W. (1979) Determination of a high-temperature transition of calcite at 800°C and one bar CO_2 pressure. Neues Jahrbuch für Mineralogie, Monatshefte, 7, 309–315.

Navrotsky, A. and Loucks, D. (1977) Calculation of subsolidus phase relations in carbonates and pyroxenes. Physics and Chemistry of Minerals, 1, 109–127.

Paul, G. L. and Pryor, A. W. (1971) The study of sodium nitrate by neutron diffraction. Acta Crystallographica, B27, 2700–2702.

Rao, C. N. R., Prakash, B., and Natarajan, M. (1975) Crystal structure transformation in inorganic nitrites, nitrates, and carbonates. National Bureau of Standards Research Data System. NSRDS-NBS, 53, 10–14.

Reeder, R. J. and Nakajima, Y. (1982) The nature of ordering and ordering defects in dolomite. Physics and Chemistry of Minerals, 8, 29–35.

Robie, R. A., Hemingway, B. S., and Fisher, J. R. (1979) Thermodynamic properties of minerals and related substances at 298.15K and at higher temperatures. Geological Survey Bulletin 1452, 302–306.

Salje, E. and Viswanathan, K. (1976) The phase diagram calcite–aragonite as derived from the crystallographic properties. Contributions to Mineralogy and Petrology, 55, 55–67.

Sanchez, J. M. and deFontaine, D. (1979) Ordering in fcc lattices with first- and second-neighbor interactions. The Physical Review, B21, 216–228.

Shockley, W. (1938) Theory of order for the copper gold alloy system. Journal of Chemical Physics, 6, 130–144.

Van Baal, C. M. (1973) Order–disorder transformations in a generalized Ising alloy. Physica (Utrect), 64, 571–586.

Manuscript received, October 25, 1982;
accepted for publication, May 24, 1983.

Appendix I

In this Appendix we derive the grand potential for a dolomite-type ordered phase in the CVM tetrahedron approximation for a trigonally distorted fcc Ising lattice of N sites.

Configurational Entropy

In general, the configurational entropy for the ordered phase is

$$S = Nk\ln\Omega_{ord} \tag{I-1}$$

where Ω_{ord} is the degeneracy factor, or number of ways of constructing the system. For an arbitrary basic cluster the CVM degeneracy factor is given by

$$\Omega = \{\text{basic cluster}\}_N^{-\gamma_{bc}} \{\text{subcluster-i}\}_N^{-\gamma_i} \ldots\ldots \{\text{points}\}_N^{-\gamma_{pts}} N!^{-\gamma_N} \tag{I-2}$$

where $\{X_{ijk\ell\ldots}\}_N \equiv \prod_{ijk\ell\ldots} (X_{ijk\ell\ldots}N)!$

and the γ factors depend upon the symmetry of the Ising lattice. In the tetrahedron approximation Eq. (I-2) becomes

$$\Omega_{tet} = \{\text{tetrahedra}\}_N^{-\gamma_{tet}} \{\text{triangles}\}_N^{-\gamma_{tri}} \{\text{pairs}\}_N^{-\gamma_{prs}} \{\text{points}\}_N^{-\gamma_{pts}} N!^{-\gamma_N} \tag{I-3}$$

We may now solve for γ factors by the method of Barker (1953) as follows:

γ_{tet} is simply the multiplicity of tetrahedra in an fcc-lattice of N sites, so that γ_{tet} = 2N-tetrahedra/N-sites = 2. The γ-factor for an arbitrary subcluster is the multiplicity of the subcluster per N sites, minus the number of times the subcluster has been implicitly counted in all larger clusters. For example, γ_{tri} = (8N triangles)/N - (2 tetrahedra) (4 triangles per tetrahedron) = 0. We note that distinguishing two types of triangles does not alter this result. Thus,

$$\gamma_1 \equiv \gamma_{tet} = 2 \tag{I-4a}$$

$$\gamma_2 \equiv \gamma_{tri} = 8 - 2(4) = 0 \tag{I-4b}$$

$$\gamma_3 \equiv \gamma_{prs} = 6 - 2(6) = -6 \tag{I-4c}$$

$$\gamma_4 \equiv \gamma_{pts} = 1 - 2(4) + 6(2) = 5 \tag{I-4d}$$

$$\gamma_5 \equiv \gamma_N = -1 \tag{I-4e}$$

where γ_N is determined by the normalization condition:

$$\sum_{i=1}^{5} \gamma_i = 0, \tag{I-5}$$

a general feature of the CVM degeneracy factor.

Before writing Ω_{ord} we must distinguish between H-pairs, Y-pairs, α-sites, and β-sites; which requires the following modifications:

$$\{\text{tetrahedron}\}_N^2 \to \{T^\alpha\text{-tet}\}_N \{T^\beta\text{-tet}\}_N \tag{I-6a}$$

$$\{\text{pairs}\}_N^6 \to \{\text{H-prs}\}_N^3 \{\text{Y-prs}\}_N^3 \tag{I-6b}$$

$$\to \{H^\alpha\text{-prs}\}_N^{3/2} \{H^\beta\text{-prs}\}_N^{3/2} \{Y^\alpha\text{-prs}\}_N^{3/2} \{Y^\beta\text{-prs}\}_N^{3/2}$$

$$\{\text{points}\}_N^5 \to \{X^\alpha\text{-pts}\}_N^{5/2} \{X^\beta\text{-pts}\}_N^{5/2} \tag{I-6c}$$

and therefore

$$\Omega_{ord} = \frac{\{H^\alpha\text{-prs}\}_N^{3/2} \{H^\beta\text{-prs}\}_N^{3/2} \{Y^\alpha\text{-prs}\}_N^{3/2} \{Y^\beta\text{-prs}\}_N^{3/2} N!}{\{T^\alpha\text{-tet}\}_N \{T^\beta\text{-tet}\}_N \{X^\alpha\text{-pts}\}_N^{5/2} \{X^\beta\text{-pts}\}_N^{5/2}} \tag{I-7}$$

Note that a full expansion of (I-7) would require substitutions of the type:

$$\{T^\alpha\text{-tet}\}_N = \{T^\alpha_{ijk\ell}\}_N \tag{I-8a}$$

$$\{H^\alpha\text{-prs}\}_N^{3/2} = \{H^\alpha_{ij}\}_N^{1/2} \{H^\alpha_{k\ell}\}_N^{1/2} \tag{I-8b}$$

etc.....

Internal Energy and Chemical Potential

We write the internal energy again in α- and β-parts as:

$$E^{\alpha} = \sum_{ijk\ell} \varepsilon_{ijk\ell} T^{\alpha}_{ijk\ell} \tag{I-9a}$$

$$E^{\beta} = \sum_{ijk\ell} \varepsilon_{ijk\ell} T^{\beta}_{ijk\ell} \tag{I-9b}$$

and the chemical potential terms are derived as follows:

$$\sum_i \mu_i N_i = \mu_1 N_1 + \mu_2 N_2 \tag{I-10a}$$

$$= (N/2) \sum_i \mu_i (x_i^{\alpha} + x_i^{\beta}) \tag{I-10b}$$

$$= (N/2) \sum \frac{1}{4}(\mu_i + \mu_j + \mu_k + \mu_\ell)[T^{\alpha}_{ijk\ell} + T^{\beta}_{ijk\ell}] \tag{I-10c}$$

$$= (N/8) \sum (\mu_i + \mu_j + \mu_k + \mu_\ell) T^{\alpha}_{ijk\ell} \tag{I-10d}$$

$$+ (N/8) \sum (\mu_i + \mu_j + \mu_k + \mu_\ell) T^{\beta}_{ijk\ell}$$

In general, $\sum_{i=1}^{n} \mu_i = 0$, for a closed system of n components and N atoms so that:

$$\mu_1 = -\mu_2 \tag{I-11}$$

Lagrange Terms

Normalization of T-variables requires

$$\sum_{ijk\ell} T^{\alpha}_{ijk\ell} = \sum_{ijk\ell} T^{\beta}_{ijk\ell} = 1 \tag{I-12a}$$

Hence,

$$\beta\lambda_{\alpha}\left(1 - \sum_{ijk\ell} T^{\alpha}_{ijk\ell}\right) = 0 \tag{I-12b}$$

$$\beta\lambda_{\beta}\left(1 - \sum_{ijk\ell} T^{\beta}_{ijk\ell}\right) = 0 \tag{I-12c}$$

and symmetry of the Y-variables requires (note indices k and ℓ)

$$\sum_j T^{\alpha}_{ijk\ell} = \sum_j T^{\beta}_{j\ell k} \tag{I-13a}$$

which leads to the Lagrange term:

$$L = L_{\alpha} + L_{\beta} = 0 \tag{I-13b}$$

where

$$L_{\alpha} = \sum_{ijk\ell} (\alpha_{i\ell} + \alpha_{j\ell} + \alpha_{k\ell}) T^{\alpha}_{ijk\ell} \tag{I-13c}$$

$$L_{\beta} = -\sum_{ijk\ell} (\alpha_{\ell i} + \alpha_{\ell j} + \alpha_{\ell k}) T^{\beta}_{ijk\ell} \tag{I-13d}$$

The Grand Potential

Applying Stirling's approximation to Eq. (I-7) and combining the result with Eqs. (I-9a), (I-9b), (I-10d), (I-12b), (I-12c), (I-13c) and (I-13d) we obtain:

$$\Phi_{ord} \equiv \hat{g}/NkT = \phi_{\alpha} + \phi_{\beta} \tag{I-16A}$$

where

$$\phi_{\alpha} = \beta\{\varepsilon_{ijk\ell} - \tfrac{1}{8}(\mu_i + \mu_j + \mu_k + \mu_\ell)\} T^{\alpha}_{ijk\ell}$$

$$+ \sum_{ijk\ell} L(T^{\alpha}_{ijk\ell}) - \tfrac{1}{2}\left[\sum_{ij} L(H^{\alpha}_{ij}) + \sum_{jk} L(H^{\alpha}_{jk}) + \sum_{ki} L(H^{\alpha}_{ki})\right]$$

$$- \tfrac{1}{2}\left[\sum_{i\ell} L(Y^{\alpha}_{i\ell}) + \sum_{j\ell} L(Y^{\alpha}_{j\ell}) + \sum_{k\ell} L(Y^{\alpha}_{k\ell})\right]$$

$$+ \tfrac{5}{8}\left[\sum_i L(X^{\alpha}_i) + \sum_j L(X^{\alpha}_j) + \sum_k L(X^{\alpha}_k) + \sum_\ell L(X^{\beta}_\ell)\right] \tag{I-16B}$$

$$+ \beta\lambda_{\alpha}\left(1 - \sum_{ijk\ell} T^{\alpha}_{ijk\ell}\right) + \sum_{ijk\ell} (\alpha_{i\ell} + \alpha_{j\ell} + \alpha_{k\ell}) T^{\alpha}_{ijk\ell}$$

and

$$\phi_{\beta} = \beta\{\varepsilon_{ijk\ell} - \tfrac{1}{8}(\mu_i + \mu_j + \mu_k + \mu_\ell)\} T^{\beta}_{ijk\ell}$$

$$+ \sum_{ijk\ell} L(T^{\beta}_{ijk\ell}) - \tfrac{1}{2}\left[\sum_{ij} L(H^{\beta}_{ij}) + \sum_{jk} L(H^{\beta}_{jk}) + \sum_{ki} L(H^{\beta}_{ki})\right]$$

$$- \tfrac{1}{2}\left[\sum_{\ell i} L(Y^{\beta}_{\ell i}) + \sum_{\ell j} L(Y^{\beta}_{\ell j}) + \sum_{\ell k} L(Y^{\beta}_{\ell k})\right] \tag{I-16C}$$

$$+ \tfrac{5}{8}\left[\sum_i L(X^{\beta}_i) + \sum_j L(X^{\beta}_j) + \sum_k L(X^{\beta}_k) + \sum_\ell L(X^{\alpha}_\ell)\right]$$

$$+ \beta\lambda_{\beta}\left(1 - \sum_{ijk\ell} T^{\beta}_{ijk\ell}\right) - \sum_{ijk\ell} (\alpha_{\ell i} + \alpha_{\ell j} + \alpha_{\ell k}) T^{\beta}_{ijk\ell}$$

where the operator $L(x) \equiv \ln x - x$.